25th ABCM International Congress of Mechanical Engineering
October 20-25, 2019, Uberlândia, MG, Brazil

COB-2019-1869
POLYGON WALL BOUNDARY MODEL IN PARTICLE-BASED METHOD: APPLICATION TO BRUMADINHO TAILINGS DAM FAILURE

Rubens Augusto Amaro Junior
Lucas Soares Pereira
Liang-Yee Cheng
Department of Construction Engineering, Polytechnic School of University of São Paulo
Av. Prof. Almeida Prado, trav. 2, 83 - Cidade Universitária, 05508-900, São Paulo, SP, Brazil
rubens.amaro@usp.br
lucas_pereira@usp.br
cheng.yee@usp.br

Ahmad Shakibaeinia
Department of Civil, Geological and Mining Engineering Polytechnique Montreal
2900, boul. Édouard-Montpetit, Montréal, Québec, Canada
ahmad.shakibaeinia@polymtl.ca

Abstract. *Recent tailings dam disasters in Brazil have increased the public concern on the risk and potential environmental damages of the existing tailings dams. The prediction of tailings slurry flow due to the dam failures is of great importance for incident prevention and mitigation. This study aims to develop a numerical model in order to predict potential damage thus assisting in a management plan to save human lives against such tailings dam failures. The numerical model is based on the mesh-free particle-based method weakly compressible moving particle semi-implicit and the explicitly represented polygon wall boundary model, in which the fluid domain is modeled by Lagrangian particles whereas solid boundaries are represented by triangular polygons. Besides the reduced computational cost, polygons are more flexible to model the surface of the complicated-shaped bodies compared with conventional particle-based representation. First, the numerical model is validated by experimental data from a 3D dam breaking problem. After that, the numerical model is applied to the Córrego do Feijão mine tailings dam failure accident. The comparison of the computed results with the known consequences shows the ability of the model to reproduce the three-dimensional dynamic behavior of the destructive tailings slurry flow that may occur on complicated terrain.*

Keywords: *tailings dam failure, disaster prevention and mitigation, numerical simulation, polygon wall boundary model, moving particle semi-implicit*

1. INTRODUCTION

Tailings dam/storage facilities are some of the largest geotechnical engineered structures on earth. Their failure accidents are generally characterized by limited emergency response times, large volumes of released materials, high velocity slurry flows and long run-out distances (Wang et al., 2018), which can often lead to serious socioeconomic impacts, irrecoverable environmental damages and losses of humans and wildlife. These accidents are dramatically increasing worldwide, and at least two major accidents annually occurred in the last 20 years (WISE, 2019).

Recent catastrophes in Brazil have increased the public concern on the risk and potential impacts of the existing tailings dams. Among the disasters that occurred after 2010, two are notable due to their severe impact on the human lives, ecosystem integrity and ecological processes. On 5 November 2015, the Fundão tailings dam, one of the megastructures of the Germano mining complex, located in the municipality of Mariana, Minas Gerais, southeastern Brazil, collapsed, releasing approximately 43 million m^3 of tailings with mud waves of more than 10 meters height. This catastrophe resulted in 19 fatalities and irreversible environmental damage to hundreds of watercourses in the Doce River basin and associated ecosystems (Carmo et al., 2017; Samarco, 2016). Based on 308 cases of mining dam collapses in the world between 1915 and 2016, the Fundão dam failure can be considered the largest technological disaster in terms of volume of tailings dumped and the geographical extension of environmental damage (Carmo et al., 2017). On 25 January 2019, the tailings dam No. 1 of Córrego do Feijão iron ore mine, situated in the municipality of Brumadinho, Minas Gerais, southeastern Brazil, suddenly failed, releasing almost its complete holdings of about 13 million m^3 of tailings. The tailings wave first destroyed an administrative area where many mining workers were having

lunch at the time. After that, an iron ore railway bridge was hit by the tailings wave, and more than 20 buildings were destroyed 3 km downstream. After flowing more than 9 km downhill, the tailings wave reached the Paraopeba River, compromising downstream areas with toxic pollution. At least 248 people died and 22 are missing as a result of this disaster.

The prediction of the main behaviors of the slurry flow post tailings dam failure is of great importance to support management decisions, as well as to provide guidelines for site plans and designs. Due to its convenience, efficiency and effectiveness in solving complex and devasting large-scale disaster problems (Vassilevski et al., 2013), as well as providing valuable information about the potential flood, the numerical simulations have been proven to be effective for such problems.

In the last decades, the mesh-free particle-based methods, such as smoothed particle hydrodynamics (SPH) (Gingold and Monagham, 1977; Lucy, 1977), and moving particle semi-implicit (MPS) (Koshizuka and Oka, 1996), opened new perspectives for the modeling of the large-scale problems involving free-surface with fragmentation and merging of liquids, and complex-shaped multi-bodies with moving and deformable boundaries. To give an illustration of that, large-scale disaster such as urban flood (Albano et al., 2016), tsunami (Murotani et al., 2017) and dam failure (Wang et al., 2018) were investigated by using particle-based methods. Within this context, the aim of the present study is to develop a particle-based numerical modeling for the simulation of the tailings slurry flow on complex terrain and evaluation of its impact, not only based on the estimation of the flood extent, but also the prediction of post tailings dam failure scenarios and more accurate assessment of the destructive potential through more complete and accurate fluid-structure interaction (FSI) modeling.

For this purpose, a numerical approach based on the weakly compressible MPS (WC-MPS) method (Shakibaeinia and Jin, 2010) is adopted. In order to provide a more efficient and effective modeling of the complex-shaped bodies, the explicitly represented polygon (ERP) wall boundary model (Mitsume et al., 2015) is implemented. In this way, in the numerical approach, the fluid domain is modeled by Lagrangian particles whereas the solid boundaries are represented by using a mesh of polygons. Compared to conventional wall particles representation, polygons are more flexible to model complicated-shaped bodies and their adoption reduces the computational cost and memory usage, therefore opening new possibilities in modeling even further large-scale phenomena such as tailings dam failures and tsunami simulations. Moreover, an axis-aligned bounding box (AABB) hierarchy is adopted to accelerate the calculation of the distances between the particles and polygons. As a result, the major contribution of our work is a practical numerical tool that enables the simulation of tailings slurry flow, providing results about its spatial and temporal evolution. Such information is crucial to predict potential impact area damages and to assist in the design process of tailings dam. For sake of simplicity, as a first step, the tailings slurry flow is modeled as a very high-viscosity Newtonian fluid and free or deformable solids are not considered. The present model is verified by comparing computed results with the known consequences of the dam break at Córrego do Feijão mine in Brumadinho, Brazil.

2. NUMERICAL METHOD

2.1 Weakly compressible moving particle semi-implicit (WC-MPS)

The moving particle semi-implicit (MPS) method is a fully Lagrangian meshfree particle-based approach. Proposed by Koshizuka and Oka (1996) for the simulation of incompressible flow with free surface, the original MPS adopts a semi-implicit algorithm to solve the governing equations of continuum by replacing the differential operators with numerical operators derived from a weight function ω_{ij}. For the problem investigated here, we assume a flow with limited compressibility and the fully incompressible model in MPS is replaced with a weakly incompressible model given by the equation of state (Shakibaeinia and Jin, 2010):

$$p_i^{t+\Delta t} = \frac{\rho c_0^2}{\gamma}\left[\left(\frac{n_i^*}{n^0}\right)^{\gamma} - 1\right], \tag{1}$$

where p_i represents the pressure of particle i, ρ is the fluid density, t is the time, $n_i^* = \sum_{i \neq j} \omega_{ij}$ is the particle number density computed after the new arrangement of particles due viscosity and external forces, see Eq. (3), n^0 is the initial particle number density for a complete support of neighbor particles, c_0 stands for the artificial speed of sound in the reference density and $\gamma = 7$ is a typical value adopted. The artificial speed of sound is usually used to avoid the instability and small time steps. In order to keep the density variations less than 1%, c_0 is chosen about ten times the maximum velocity, according to Monaghan (1994).

At first, predictions of the particle's velocity ($\mathbf{u}_i$) and position ($\mathbf{r}_i$) vectors are carried out by using viscosity and external forces terms of the momentum conservation:

$$\mathbf{u}_i^* = \mathbf{u}_i^t + \frac{(\nu_k \langle \nabla^2 \mathbf{u} \rangle_i + \mathbf{f}_i)\Delta t}{\rho}, \tag{2}$$

$$\mathbf{r}_i^* = \mathbf{r}_i^t + \mathbf{u}^t \Delta t, \tag{3}$$

where ν_k represents the kinematic viscosity and **f** is the external body force per unit mass vector. $\langle\ \ \rangle$ symbolizes the numerical operators of the MPS method.

After the calculation of the pressures by Eq. (1), the velocity and position of the particles are updated by using the pressure gradient term of the momentum conservation:

$$\mathbf{u}_i^{t+\Delta t} = \mathbf{u}_i^* - \frac{\langle \nabla P \rangle_i \Delta t}{\rho}, \tag{4}$$

$$\mathbf{r}_i^{t+\Delta t} = \mathbf{r}_i^* + \mathbf{u}_i^{t+\Delta t} \Delta t. \tag{5}$$

The Dirichlet pressure boundary condition is imposed to the particles identified as free surface. A particle is defined as free-surface one and its pressure is set to zero when its particle number density n_i^* is smaller than n^0.

2.2 Polygon wall boundary model

The explicitly represented polygon (ERP) wall boundary model (Mitsume et al., 2015) was used to model the solid boundary. The ERP model represents solid boundaries as triangular polygons in an explicit way without using distance functions. Moreover, the creation of neighbor virtual particles or special adaptations for angled edges are not required. The pressure Neumann boundary condition and the slip/no-slip condition on the walls are satisfied. Compared to fully particle-based representation, the ERP wall boundary model has advantages such as (Mizuno et al., 2018):

- triangular polygons are more flexible to model the surface of the complicated-shaped rigid bodies,
- computational cost can be reduced because wall and dummy particles are not required,
- Newton's third law is assured at the interface between fluid and solid. Therefore, higher accuracy and stability are expected.

An axis-aligned bounding box (AABB) hierarchy, implemented using the C++ library libigl (Jacobson et al., 2018), is adopted in the present study to accelerate the calculation of the distances between the particles and polygons.

Since the solid walls are represented by polygons in the ERP model, the compact support of fluid particles near the walls is not fully filled with particles. Hence, the numerical operators of these particles are divided into the contribution due fluid particles $\langle\ \ \rangle^{particle}$ and polygon walls $\langle\ \ \rangle^{wall}$, as illustrated in Fig. 1. To calculate the numerical operators $\langle\ \ \rangle^{wall}$, first, the position of the mirror particle i' corresponding to particle i is computed. After that, the numerical operators of particle i' are computed considering the original particle i and its neighbors inside the neighbor region of i'. Finally, these operators are transformed, by the multiplication of the transformation matrix $\mathbf{R}_i^{ref}$ or $\mathbf{R}_i^{inv}$, and are added to the numerical operators $\langle\ \ \rangle^{particle}$ of particle i.

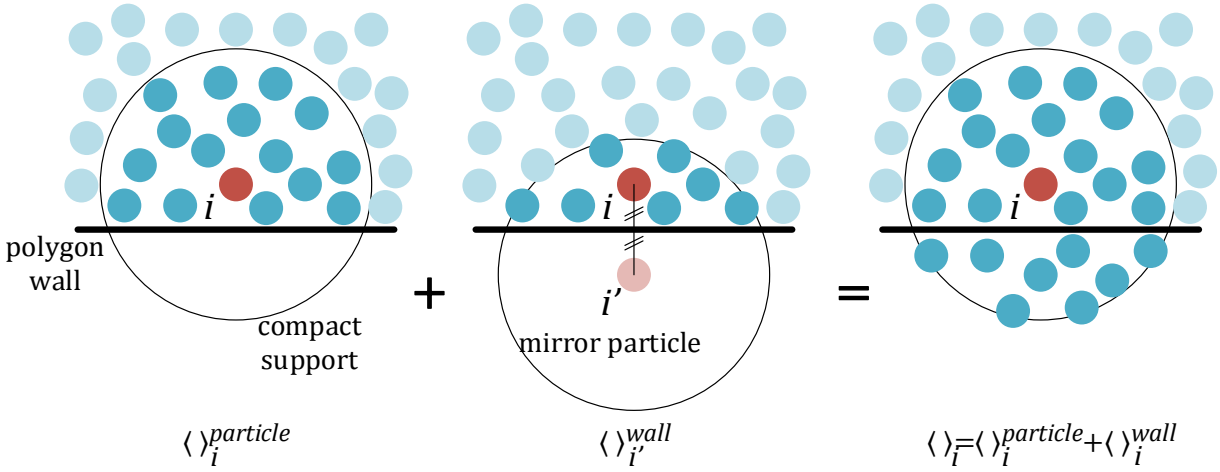

Figure 1. ERP model. Contribution of fluid particles and polygon walls to the calculation of numerical operators

The pressure gradient and the Laplacian of the velocity terms are calculated as:

$$\langle \nabla P \rangle_i = \langle \nabla P \rangle_i^{particle} + \langle \nabla P \rangle_i^{wall}, \tag{6}$$

$$\langle \nabla^2 \mathbf{u} \rangle_i = \langle \nabla^2 \mathbf{u} \rangle_i^{particle} + \langle \nabla^2 \mathbf{u} \rangle_i^{wall}, \tag{7}$$

where $\langle\ \ \rangle^{particle}$ denotes the contribution of fluid particles in the same way of the original MPS (Koshizuka and Oka, 1996). The operators $\langle\ \ \rangle^{wall}$ for the pressure gradient and Laplacian of the velocity for the no-slip boundary condition are computed as (Mitsume et al., 2015):

$$\langle \nabla P \rangle_i^{wall} = \mathbf{R}_i^{ref} \frac{d}{n^0} \sum_{j \in \Omega_{i'}} \left(P_j + P_i - 2\bar{P}_i \right) \frac{(\mathbf{r}_j - \mathbf{r}_{i'})}{|\mathbf{r}_j - \mathbf{r}_{i'}|^2} \omega_{i'j}, \tag{8}$$

$$\langle \nabla^2 \mathbf{u} \rangle_i^{wall} = \mathbf{R}_i^{inv} \frac{2d}{\lambda^0 n^0} \sum_{j \in \Omega_{i'}} \left(\mathbf{u}_j - \mathbf{u}_{i'} \right) \omega_{i'j}, \tag{9}$$

where d is the number of spatial dimensions and $\omega_{i'j}$ is the weight function between the neighbor particles j and the mirror particle i':

$$\omega_{i'j} = \begin{cases} \frac{r_e}{|\mathbf{r}_{i'j}|} - 1 & |\mathbf{r}_{i'j}| \le r_e \\ 0 & |\mathbf{r}_{i'j}| > r_e \end{cases}, \tag{10}$$

where r_e is the effective radius, here assigned to $2.1l_0$, where l_0 is the initial distance between two particles. $\lambda^0 = \sum_{j \neq i} \omega_{ij}^0 |\mathbf{r}_{ij}^0|^2 / \sum_{j \neq i} \omega_{ij}^0$ is a correction parameter computed at the initial of the simulation for a complete support of neighbor particles. $\bar{P}_i$ is the minimum pressure within the effective radius r_e.

The position of the mirror particle i' corresponding to particle i is obtained as:

$$\mathbf{r}_{i'} = \mathbf{r}_i + 2\left(\mathbf{r}_i^{wall} - \mathbf{r}_i \right), \tag{11}$$

where $\mathbf{r}_i^{wall}$ is the closest point on the polygon to particle i.

The transformation matrix for reflection across the plane $\mathbf{R}_i^{ref}$, whose unit normal vector at the position of particle i is $\mathbf{n}_i^{wall}$, and the inverse transformation matrix $\mathbf{R}_{inv}$ are expressed as:

$$\mathbf{R}_i^{ref} = \mathbf{I} + 2\mathbf{n}_i^{wall} \otimes \mathbf{n}_i^{wall}, \tag{12}$$

$$\mathbf{R}^{inv} = -\mathbf{I}, \tag{13}$$

where $\mathbf{I}$ is the identity matrix.

The Eq. (9) represents the Laplacian of velocity for the no-slip boundary condition on a wall whose velocity of the mirror particle is:

$$\mathbf{u}_{i'} = \mathbf{R}^{inv} \left\{ \mathbf{u}_i - 2\left[\mathbf{u}_i^{wall} - \left(\mathbf{n}_i^{wall} \cdot \mathbf{u}_i^{wall} \right) \mathbf{n}_i^{wall} \right] \right\}, \tag{14}$$

where $\mathbf{u}_i^{wall}$ is the velocity of the wall at the point at which it is acted on by the force of particle i.

A repulsive force $\mathbf{f}_i^{rep}$ is added to Eq. (8) to prevent penetrations of the fluid particles at curved edges of the bodies:

$$\mathbf{f}_i^{rep} = \begin{cases} -\alpha_{rep} \left(\frac{0.5 l_0}{|\mathbf{r}_{ij}|} - 1 \right) \mathbf{n}_i^{wall} & |\mathbf{r}_{ij}| \le 0.5 l_0 \\ 0 & |\mathbf{r}_{ij}| > 0.5 l_0 \end{cases}, \tag{15}$$

where α_{rep} is a repulsive coefficient empirically determined.

The particle number density n_i also is partitioned into the contribution due the fluid particles $n_i^{particles}$ and the polygon walls n_i^{wall}. Under the assumption that the wall near the fluid particle is flat, the dummy particles j' are arranged in a uniform particle distribution below the flat wall, and n_i^{wall} is evaluated using the dummy particles as:

$$n_i^{wall} = f(d_{iwall}) = \sum \omega_{ij'}, \tag{16}$$

where f is determined by a linear interpolation of precomputed values at a given discrete distance d_{iwall}, the normal distance between the particle i and the nearest polygon wall. It should be emphasized that $\omega_{ij'}$ is computed at a few points within the effective radius r_e at the beginning of the simulation and are stored in a lookup table, then saving the processing time.

3. VALIDATION OF THE NUMERICAL METHOD

A dam breaking experiment performed by Lobovský et al. (2014) was numerically reproduced to validate the numerical method. The column water and main dimensions of the 3D rectangular tank are shown in Fig. 2. In the numerical simulation, the gate is not modeled because it is assumed a sudden removal of the gate

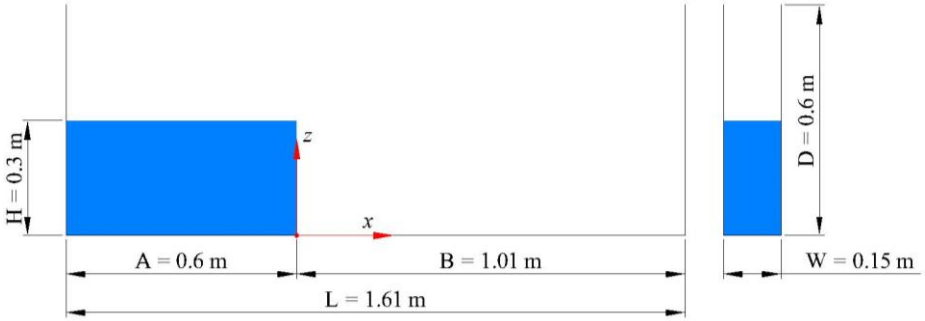

Figure 2. Main dimensions of the 3D dam breaking

The fluid was modeled with the same characteristics of the experiment, i.e., density of 997 kg/m^3 and kinematic viscosity of $8.9 \times 10^{-7} m^2/s$. Four initial distances between particles were considered: $l_0 = 30\ mm$, $l_0 = 15\ mm$, $l_0 = 7.5\ mm$ and $l_0 = 3.75\ mm$, corresponding to the resolutions of $H/l_0 = 10$, $H/l_0 = 20$, $H/l_0 = 40$ and $H/l_0 = 80$, respectively. The number of particles, the estimated time required for a simulation of 1 s and the repulsive coefficient (α_{rep}), empirically determined for each resolution, are presented in Table 1. The artificial speed of the sound was adopted as $c_0 = 10v = 10\sqrt{2gH} \cong 25\ m/s$ for all resolutions.

Table 1. Dam breaking. Numerical parameters, approximate number of particles and computational cost

Distance between particles (l_0)[mm]	30	15	7.5	3.75
Resolution (H/l_0)	10	20	40	80
Number of particles	1000	8000	64000	512000
Time step [ms]	0.5	0.2	0.1	0.05
Computational time† [min]	0.3	8.0	98.0	1740.0
Repulsive coefficient (α_{rep}) [N/m³]	200000	500000	1000000	5000000

†CPU Intel® Core™ Processor i7-4790, processor base frequency of 3.60 GHz, 4 cores and 16 GB of memory

Figure 3 presents the comparison between the experimental (Lobovský et al., 2014) and computed wave fronts for all resolutions. In order to compare the experimental results, the propagation of the wave front x is non-dimensionalized against the initial filling height H in the dam reservoir as $x' = x/H$. The experimental data are plotted versus the non-dimensional time $t^* = t\sqrt{g/H}$, where t represents the dimensional time measured since the start of the gate's vertical motion, and g is the gravity acceleration. The increase of the resolution leads to a slight increase of the velocity of the wave front, and the computed wave front propagations show good agreements with the experimental one, even for the low-resolution of $H/l_0 = 10$.

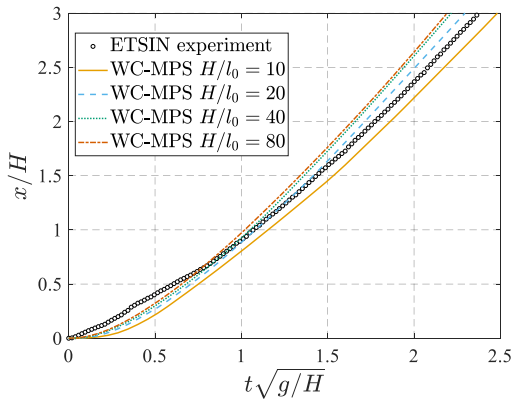

Figure 3. Comparison between the experimental (Lobovský et al., 2014) and computed wave front for four resolutions

4. RESULTS AND DISCUSSION

4.1 Numerical model

In the present study, the real-scale 3D geometry of the surrounded area of the Córrego do Feijão tailings dam disaster was modeled based on the global 1 arc-second (30 m along the equator) data from Shuttle Radar Topography Mission (SRTM) digital elevation model (USGS, 2019). The SRTM elevation models are arranged into tiles, each covering one degree of latitude and one degree of longitude, named according to their south western corners.

Figure 4(a) shows the visualization of the elevation model of the region S21W045, where the dam break and debris flow analyzed in this work occurred. Using the QGIS software the SRTM file, provided as tagged image file (tif) format, can be visualized and saved as stereolithography (stl) file. The saved stl file covers only the directly affected region, from the Córrego do Feijão dam until Paraopeba river, resulting an approximated area of 5.9 x 5.2 km. The particles for simulation of the dam break was generated using the model showed in Fig. 4(b). The geometry of the tailings dam was modeled according to the available images and observing its volume of approximately 13 million m^3 and height of 87 m.

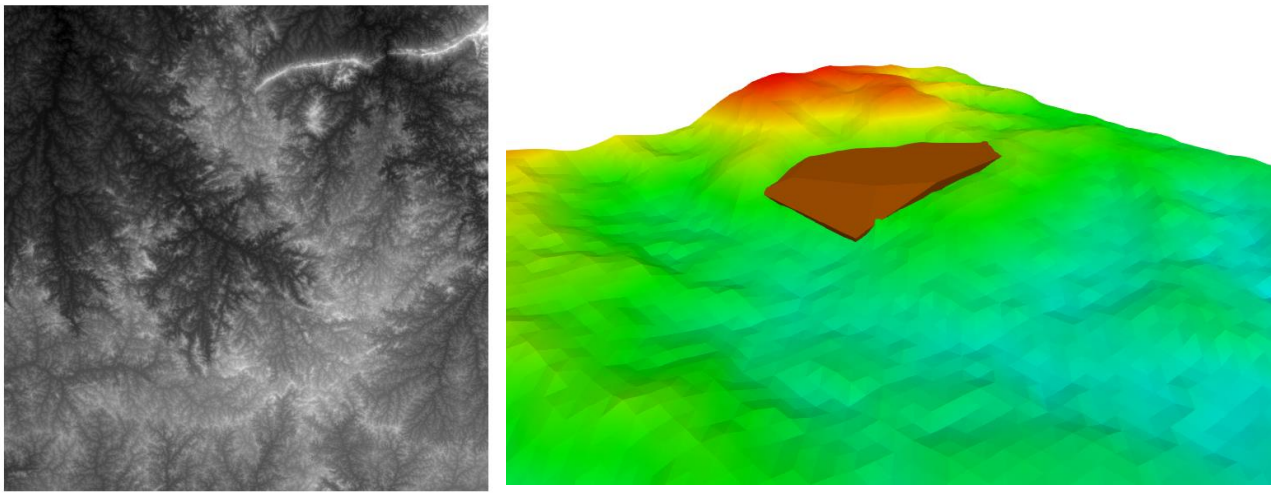

Figure 4. TIF (left) and STL (right) files of the terrain and fluid

The initial geometry and simulation at the instant t = 100 s are shown in Fig 5. Here, as a first attempt, the slurry was considered as a mixture of water and a high concentration of iron ore and simplified by a single-phase flow of Newtonian fluid, i.e., the actual rheological parameters were not considered. The following parameters were adopted: density of the iron ore $p_s = 3000$ kg/m^3, density of water $p_w = 1000$ kg/m^3, density of the slurry mixture, with a solid concentration $C_w = 50\%$, $\rho_m = 100/[C_w/\rho_s + (100 - C_w)/\rho_w] = 1500$ kg/m^3, kinematic viscosity ν = 3.0 m^2/s and gravitational acceleration g = 9.81 m/s^2. Considering the time between the initial instant of the tailing dam collapse and the arrival of the slurry in the Paraopeba River, approximately 3 hours as reported in G1 (2019), the physical time of the simulation was set to t = 10000 s. The simulation parameters are presented in Table 2.

Table 2. Córrego do Feijão tailings dam disaster. Simulation parameters

Distance between particles (l_0)[m]	10	5
Number of particles	12713	101822
Triangular elements size (Δx) [m]	40	40
Number of elements	46125	46125
Time step [s]	0.02	0.01
Computational time†	5h15m	2d20h00m
Repulsive coefficient (α_{rep}) [N/m³]	100000	100000
Sound speed c_0 [m/s]	400	400

†CPU Intel® Core™ Processor i7-8700, processor base frequency of 3.20 GHz, 6 cores and 16 GB of memory

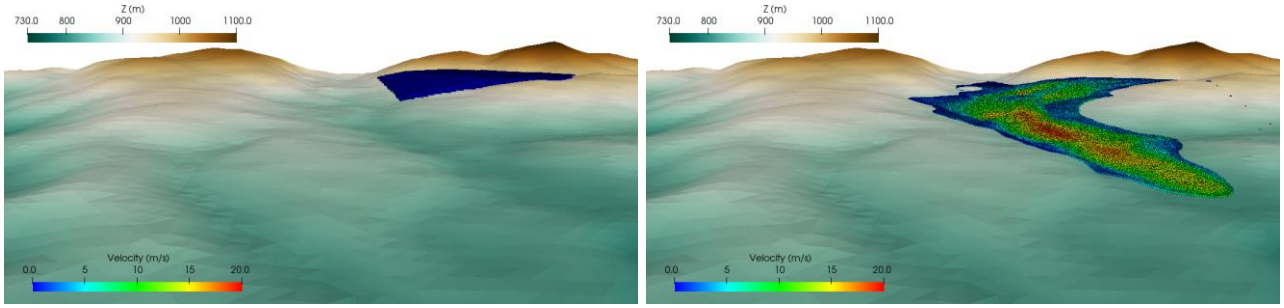

t = 0 s t = 100 s

Figure 5. Initial instant t = 0 s (left) and simulation at the instant t = 100 s (right)

4.2 Analisys of the results

Figure 6 shows the snapshots of the flooded area numerically computed by the present model. The red color indicates the flooded area computed using $l_0 = 10\ m$ while the blue one portrays the simulation result using $l_0 = 5\ m$. As a reference, the satellite image of the affected area (DigitalGlobe, 2019) is used as the texture on the surface mesh. After the tailings dam collapse, the toxic mud flows downhill in both simulations and flooded the administrative area 1 km away from the dam, at the instant t = 60 s. After that, a large area is submerged by the slurry and the front wave progress towards the Railway bridge at t = 120 s, reaching a distance about 3 km downstream for the case with $l_0 = 10\ m$ and 2 km downstream for the $l_0 = 5\ m$. A significant reduction on the flow velocity occurs after t = 120 s, and the flow approaches a farmland around 5 km downstream, at t = 1800 s. After flowing more than 6 km downward, the flow becomes more stable reaching a residential area at t = 3600 s. At the instant t = 9000 s, the flow towards the Paraopeba River 8 km away for the simulation with $l_0 = 5\ m$, whereas the flow propagation decreases remarkably for $l_0 = 10\ m$.

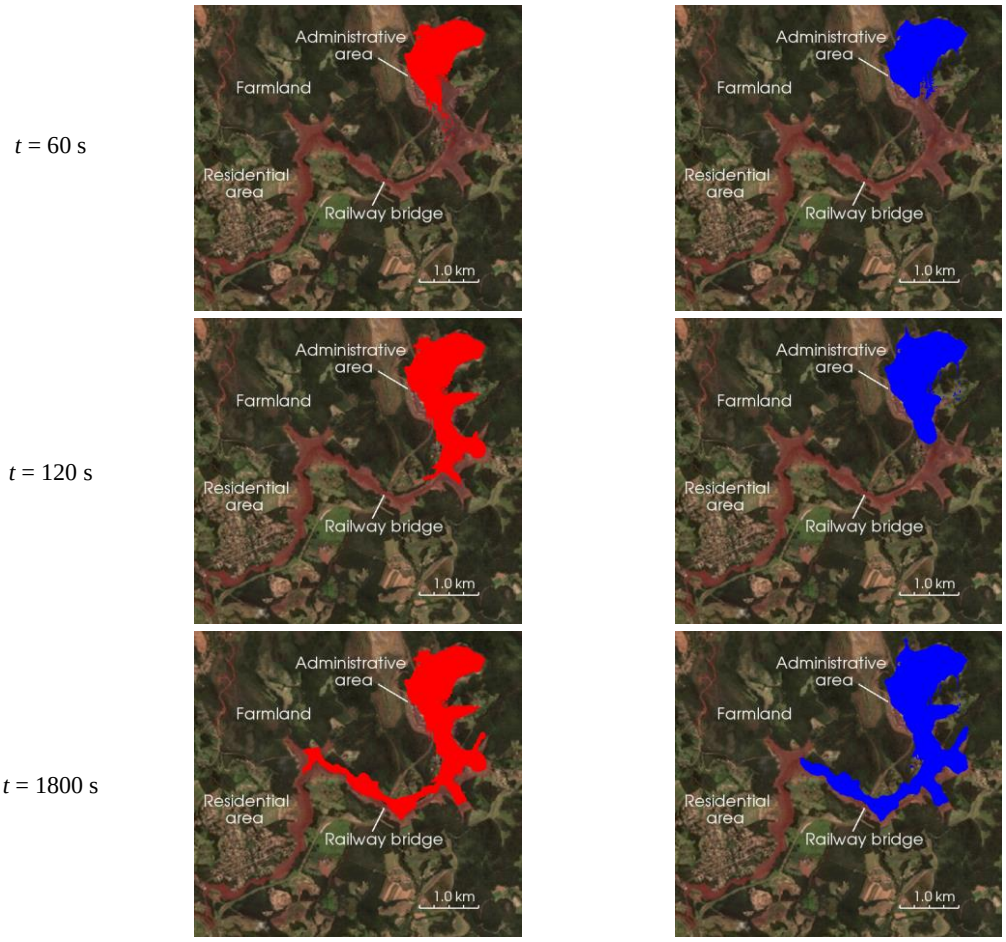

t = 60 s

t = 120 s

t = 1800 s

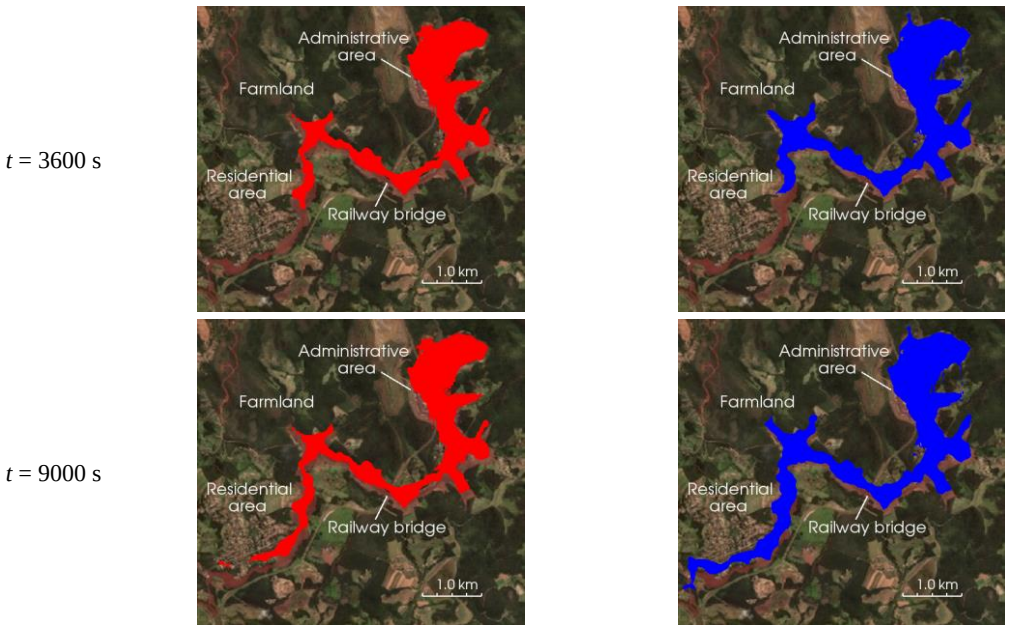

(a) $l_0 = 10$ m (b) $l_0 = 5$ m

Figure 6. Snapshots of the 3D slurry flow. Simulation with particle distance (a) $l_0 = 10$ m and (b) $l_0 = 5$ m

Figure 7 gives the wave front progress of the slurry flow along the time. After the tailings dam collapse, the flow follows a same trend approximately until t = 5000 s, for both distances of particles. However, during the first 5000 seconds, the wave front propagation computed for $l_0 = 10$ m is faster than the computed one for $l_0 = 5$ m, and the slurry flow reached about 6.8 km away from the dam for $l_0 = 10$ m whereas the distance traveled for $l_0 = 5$ m is about 6.4 km. After t = 5000 s, the wave front velocity computed for $l_0 = 10$ m is remarkably reduced, and the wave front becomes to calm down reaching the distance around 7.2 km, although some fluid particles continues to move towards the Paraopeba River, as depicted in Fig. 6(a), t = 9000 s. The wave front continues to flow for the simulation with $l_0 = 5$ m reaching the distance about 8.4 km downstream, after t = 5000 s, and flowing towards the Paraopeba River, matching reasonably well with the real events reported in G1 (2019).

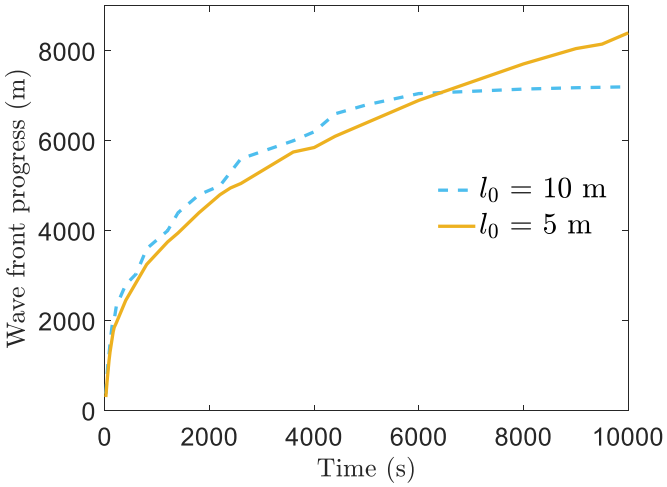

Figure 7. Propagation of the slurry flow for particle distances $l_0 = 10$ m (dashed line) and $l_0 = 5$ m (solid line)

Overall, the numerically computed slurry flow directions and impacted area are in agreement with the actual ones, despite some local differences. Besides the adoption of a Newtonian fluid and neglecting the land surface roughness, such differences also might be attributed to the coarser resolution so that some fine topographic details and fluid behavior were lost in the numerical modeling. The preliminary comparison indicates that the present model provides acceptable results for practical purposes, although simulations with high-resolution models and non-Newtonian fluid are recommended.

5. CONCLUSIONS

A 3D numerical model based on the MPS method has been developed for the modeling of the dynamic of tailings slurry flow. In order to reduce the computational cost, the ERP wall boundary model was adopted. Qualitative comparisons between the numerically computed results with the known consequences of the Córrego do Feijão tailings dam failure and quantitative comparisons between the computed wave front progress were carried out. Overall good agreement showed the effectiveness of the present approach to reproduce the three-dimensional dynamic behavior of the destructive tailing slurry flow over complicated terrain. The present model can be used as a practical tool for the mitigation and emergency management plan of tailings dam disasters. However, further improvements of the rheological model, surface roughness and computational performance are desirable. Moreover, future work is needed to take advantage of the particle-based method for the modelling of local regions of interesting, where complex fluid-solid interaction may occurs, while using mesh-based method for the modelling of the remain domain to save the processing time and computer storage. In this way, future extensions of the numerical model will provide a flexible tool suitable for FSI problems such as free surface flows interacting with multiple bodies, which is a challenge for two-dimensional mesh-based models.

6. ACKNOWLEDGEMENTS

Authors would like to thank Mr. Alec Jacobson for providing the open-source C++ library libigl. Authors also would like to acknowledge the Coordenação de Aperfeiçoamento de Pessoal de Nível Superior - Brasil (CAPES), and Conselho Nacional de Desenvolvimento Científico e Tecnológico (CNPq) for providing scholarship support for the first and second authors, respectively.

7. REFERENCES

Albano, R., Sole, A., Mirauda, D. and Adamowski, J., 2016. "Modelling large floating bodies in urban area flash-floods via a smoothed particle hydrodynamics model". *Journal of Hydrology*, Vol. 541, pp. 344-358.

Carmo, F.F., et al., 2017. "Fundão tailings dam failures: the environment tragedy of the largest technological disaster of Brazilian mining in global context". *Perspectives in Ecology and Conservation*, Vol. 15, No. 3, pp. 145-151.

DigitalGlobe, 2019. "Satellite imagery" 26 Mar. 2019. <https://discover.digitalglobe.com/>.

G1, 2019. "Tragédia em Brumadinho: animação mostra ponto a ponto o deslocamento do mar de lama; VÍDEO" 26 Mar. 2019 <https://g1.globo.com/mg/minas-gerais/noticia/2019/01/31/tragedia-em-brumadinho-animacao-mostra-ponto-a-ponto-o-deslocamento-do-mar-de-lama-video.ghtml>.

Gingold, R. A. and Monaghan, J. J., 1977. "Smoothed particle hydrodynamics: theory and application to non-spherical stars." *Monthly Notices of the Royal Astronomical Society*. Vol. 181, pp. 375-389.

Jacobson, A., Panozzo, D. and others, 2018 "libigl: A simple C++ geometry processing library" 26 Mar. 2018 <http://libigl.github.io/libigl/>

Koshizuka, S. and Oka, Y., 1996. "Moving particle semi-implicit method for fragmentation of incompressible fluid". *Nuclear Science and Engineering*, Vol. 123, No. 3, pp. 421-434.

Lobovský, L. et al., 2014. "Experimental investigation of dynamic pressure loads during dam break". *Journal of Fluids and Structures*, Vol. 48, pp. 407-434.

Lucy, L., 1977. "A numerical approach to the testing of the fission hypothesis." *Astronomical Journal*, Vol. 82, pp. 1013-1024.

Mitsume, N., Yoshimura, S., Murotani, K. and Yamada, T., 2015. "Explicitly represented polygon wall boundary model for the explicit MPS method". *Computational Particle Mechanics*, Vol. 2, No. 1, pp. 73-89.

Mizuno, Y., Mitsume, N., Yamada, T. and Yoshimura, S., 2018. "Fluid-rigid body interaction analysis for mesh-free particle method with polygon boundary representation". *Theoretical and Applied Mechanics Japan*, Vol. 64, pp. 133-142.

Monaghan, J. J., 1994. "Simulating Free Surface Flows with SPH." *Journal of Computational Physics*, Vol. 110, No. 2, pp. 399-406.

Murotani, K., et al., 2017. "Development of hierarchical domain decomposition explicit MPS method and application to large-scale tsunami analysis with floating objects". *Journal of Advanced Simulation in Science and Engineering*, Vol. 1, No. 1, pp. 16-3.

Samarco, 2016. “Samarco relatório sobre as causas imediatas da ruptura da barragem de fundão” 26 Mar. 2019 <http://fundaoinvestigation.com/wpontent/uploads/general/PR/pt/FinalReport.pdf>.

Shakibaeinia, A. and Jin, Y.-C., 2010. “A weakly compressible MPS method for modeling of open-boundary free-surface flow”. *International Journal for Numerical Methods in Fluids*, Vol. 63, No. 10, pp. 1208-1232.

USGS, 2019. United States Geological Survey. 26 Mar. 2019 < http://earthexplorer.usgs.gov/>.

Vassilevski, Y., Nikitin, K., Olshanskii, M., and Terekhov, K.V., 2013. “CFD technology for 3D simulation of large-scale hydrodynamic events and disasters”. *Russian Journal of Numerical Analysis and Mathematical Modelling*, Vol. 27, No. 4, pp. 399-412.

Wang, K., Yang, P., Hudson-Edwards, K.A., Lyu, W., Yang, C. and Jing, X., 2018. “Integration of DSM and SPH to model tailings dam failure run-out slurry routing across 3D real terrain”. *Water*, Vol. 10, No. 8, pp. 1-15.

WISE, 2017. “World Information Service on Energy - Chronology of major tailings dam failures”. 26 Mar. 2019 <http://www.wise-uranium.org/mdaf.html>.

8. RESPONSIBILITY NOTICE

The authors are the only responsible for the printed material included in this paper.